Effects of Surface Area and Sediment Mineralogy on Microbially Mediated Changes in Divalent Metal Speciation

A.L. Neal,[1] D. Brewe,[2] D.C. Cooper[3]
[1]Department of Microbiology, University of Georgia, Athens, GA, U.S.A.
[2]Advanced Photon Source (APS), Argonne National Laboratory (ANL), Argonne, IL, U.S.A.
[3]Idaho National Engineering and Environmental Laboratory (INEEL), Idaho Falls, ID, U.S.A

Introduction

These experiments are designed to provide an understanding of how microbial Fe^{III} reduction in an iron-bearing, clayey sediment alters sediment iron chemistry and of its subsequent effect on metallic contaminants. In order to avoid complications associated with dissimilatory metal-reducing bacteria (DMRB)-induced changes in clay mineral structure, we chose to employ a sediment with its clay mineralogy dominated by kaolinite and its iron chemistry dominated by iron oxide minerals. We also sought to avoid complications associated with redox reactive metals during this initial study and chose Zn^{II} as a model contaminant. Zn^{II} was preferred over other transition metals because it (a) is not sensitive to redox changes, (b) has an ionic diameter similar to that of iron, (c) is relatively soluble at a pH of ~7, (d) does not form strong aqueous complexes in "typical" groundwater, (e) has well-defined sorption chemistry with a variety of mineral surfaces, (f) has a cation exchange selectivity coefficient similar to that of Ca^{2+}, and (g) forms a number of carbonate minerals at elevated pCO_2 and circumneutral pH. The combination of sorption reactions (cation exchange, surface complexation with iron oxides, carbonate precipitation) was of particular interest, since microbial iron reduction would be expected to notably alter all three of these sorption mechanisms.

Methods and Materials

Shewanella putrefaciens strain 200, a facultative anaerobe, was used in these experiments under suboxic conditions ($[O_2]_{(aq)} < 2.5$ μmol L^{-1}) in an artificial groundwater (AGW) medium. The anaerobic AGW medium and synthetic very high surface area (VHSA) goethite used in these experiments were described previously [1]. The VHSA goethite was prepared as described elsewhere [2]. Sediment MNC-71 was collected from iron-bearing, clayey sediments in Marshall, North Carolina. Sufficient sediment to account for 1 mmol of citrate dithionite extractable iron (about 0.09 g of goethite, 1.3 g of MNC-71 per tube) was added to each culture. The initial culture optical density (A_{600}) was 0.020, corresponding to approximately 2×10^6 cells mL^{-1}. Fluorescence yield Zn K edge x-ray absorption spectroscopy (XAS) measurements were made at room temperature on sediment samples removed from Balch tubes and prepared under an anaerobic atmosphere. A Si(111) double-crystal monochromator was used to select x-ray energies for step scans through the Zn K edge. Harmonics in the beam were minimized by detuning the second crystal until the intensity was reduced by approximately 30% from the maximum produced by the monochromator. An ionization chamber was used to monitor the incident x-rays, and a 13-element Ge solid-state detector was used to collect the Zn fluorescence. Al and Cu filters were placed in front of the detector, thereby reducing the background due to Fe fluorescence and elastically scattered and Compton-scattered x-rays, respectively. Data were collected across the Zn K edge region at a step size of 0.8 eV. In the extended x-ray absorption fine structure (EXAFS) region, the absorption step size was 0.05 $Å^{-1}$. Data analysis was performed with Athena and Artemis in the IFEFFIT software package. Standard techniques were used to normalize the absorption spectra to the edge jump, and the Autobk algorithm was used to extract the EXAFS oscillations from the smooth background. Fitting of the near-neighbor coordination shell was performed in *R*-space after Fourier-transforming the EXAFS with k^3 weighting over a range from 0.5 to 9 $Å^{-1}$ with a 2-$Å^{-1}$ Kaiser-Bessel weighting at the spectrum end. Theoretical standards used in the fitting procedures and EXAFS background subtraction were generated by FEFF7.

Results

The results of the XAFS data analysis are illustrated in Fig. 1 and Table 1. Figure 1 shows the x-ray absorption near-edge structure (XANES). k^3-weighted Fourier transforms (FTs) (not corrected for phase shift) were obtained over a *k*-range of 0.5-9 $Å^{-1}$, with a 2-$Å^{-1}$ Kaiser-Bessel window deemphasizing the end of the data where the signal-to-noise ratio is smaller. Table 1 shows results of fitting the first-neighbor shell in *R*-space. Fitting was performed over a range of 0.5-2.0 Å with a Kaiser-Bessel window of 0.1 Å. The limited data available required that the constraints on the number of floating variables remain within the limits dictated by the number of independent data points. Reasonable results for the goethite systems and the sterile MNC-71 system were obtained with a model consisting of subshells of oxygen atoms whose

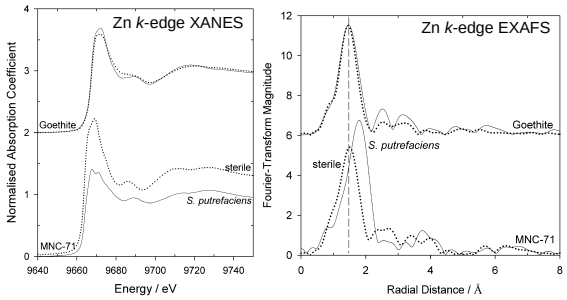

FIG. 1. Zn K edge XANES (left) and Fourier-transformed EXAFS (right) of sterile and inoculated goethite and MNC-71 sediment.

coordination numbers were fixed at a ratio of 2:1, while total coordination ($N = N_a + N_b$) was varied. *R* of each subshell was allowed to vary, as were a common E_0 and a common σ^2. Fits with individually varying σ^2's were also attempted, as were fits with other ratios of N_a and N_b, but the calculated uncertainties and the goodness-of-fit parameter χ^2_ν were degraded (these results are not shown). A realistic model for the MNC-71 system in the presence of *S. putrefaciens* could not be found (see Fig. 1).

In the case of goethite, *S. putrefaciens* has relatively little effect on the Zn coordination. The XANES is quite similar under both sterile and inoculated conditions: a white line of ~1.6 to 1.7, and the first "bump" at the same energy, ~9685 eV. Since the XANES features are a result of multiple-scattering resonances, strongly dependent on both the identity and geometry of nearby atoms, this similarity indicates the Zn environments are also similar. The first-neighbor shell in the FT is also quite similar in both position and size. There are differences in the FTs beyond the first-neighbor peak, with the sterile sample perhaps possessing increased order. On the other hand, in the case of the MNC-71 system, it is clear from both the XANES and the FTs that the presence of bacteria has a significant effect on the Zn-bonding environment. The white line in the sterile MNC-71 sample is of similar intensity (~1.7) to the intensities of the goethite samples, whereas the white line in the presence of *S. putrefaciens* is less intense but broader, exhibiting a distinctive double peak. The FTs of the two MNC-71 samples are also distinctly different from one another. The near-neighbor peak in the sterile sample is similar to those of the goethite samples, whereas the near-neighbor peak in the sample inoculated with *S. putrefaciens* is larger, broader, and shifted to larger R by ~0.3 Å. Thus, the influence of bacteria upon the Zn coordination is seen to be significantly greater in the MNC-71 system than goethite.

The fitting results shown in Table 1 broadly support the conclusions reached by examining the XANES and FTs, indicating that the precipitated Zn environment is similar in the goethite systems and the sterile MNC-71 system. There is a slight difference between the goethite samples in the results for N, but they are barely the same within

TABLE 1. Results of fitting in R-space of the first-neighbor shell. Uncertainties in the fitted parameters are shown in parentheses. Fitting was performed with Na constrained to be Nb × 2. E_0 and σ^2 were constrained to be equal for each subshell. χ^2_ν is defined as χ^2 divided by the difference between the number of independent points in the data and the number of quantities varied in the fit: $\chi^2/(N_{ind} - N_{var})$. A shows results of fitting O first neighbors to the sterile and inoculated goethite samples and sterile MNC-71. B shows results of fitting Cl or O first neighbors for inoculated MNC-71. ΔR is the difference in the fitted distance compared to the standard. Standard for the Zn-Cl model was a fourfold Zn-Cl shell with a bond length of 2.28 Å, based on $ZnCl_2$. The Zn-O standards were two shells with fourfold and twofold coordination and a bond length of 2.11 Å (total N = 6), based on $ZnCO_3$. The 0.5-9 fitting condition is the same as the one that produced the results for the other samples.

A. Sample	**$N = N_a + N_b$**	**ΔE_0 (eV)**	**R_a (Å)**	**R_b (Å)**	**σ^2 ($\times 10^{-3}$ Å^2)**	**χ^2_ν**
Goethite	4.9 (0.6)	-5.2 (1.5)	2.03 (0.01)	1.89 (0.04)	4.2 (4.0)	5.9
Goethite + *S. putrefaciens*	6.2 (0.7)	-3.9 (1.3)	2.07 (0.02)	1.94 (0.08)	9.1 (7.0)	2.9
MNC-71	5.3 (0.6)	-4.5 (1.9)	2.05 (0.01)	1.89 (0.03)	3.1 (2.9)	7.1
B. Model/FittingRange	**$N = N_a + N_b$**	**ΔE_0 (eV)**	**ΔR_a**	**ΔR_b**	**σ^2($\times 10^{-3}$A^2)**	**χ^2_ν**
Zn-Cl/3-11	5.0(1)	2.1(2.3)	0.01(0.02)	-	10.2(2.2)	16
Zn-O/3-11	5.0(1.7)	21.1(3.1)	0.06(0.02)	-	5.0(3.5)	54
Zn-O/0.5-9	4.3(1.8)	17.4(3.7)	0.03(0.03)	-	3.1(5.5)	362
Zn-O 2:1 split/3-11	4.0(1.3)	11.1(3.9)	0.07(0.03)	-0.08(0.04)	-3.1(3.2)	59
Zn-O 2:1 split/0.5-9	3.3(1.2)	9.2(4.0)	0.05(0.04)	-0.12(0.06)	-7.4(.005)	333

the uncertainties obtained from the fitting procedure. It should be noted that the fitting results reflect the difficulty in modeling a fairly complicated structure with a limited data set. In particular, note the large uncertainties in σ^2 and R, which are produced by the large correlation between these variables in a two-shell fit (the *k*-dependent beating produced by two closely spaced shells mimics the behavior of the Gaussian factor in which σ^2 appears). However, N was obtained with reasonable certainty because the fit included small *k* values, in which the effect of σ^2 is small and the two shells are nearly in phase. The results for N were also relatively insensitive to the details of the model (changing by less than 10% in each case when independent σ^2's were used for the two subshells). Overall, the fitting results, in combination with the qualitative comparison of the XANES and FTs, produce confidence in the conclusion that the immediate Zn environment in the goethite and sterile MNC-71 samples is very similar.

The attempt to model Zn local structure in the MNC-71 sample in the presence of *S. putrefaciens* also supports the conclusion reached from examining the XANES and FTs that Zn coordination is significantly different from the others. In this case, a reasonable model with oxygen neighbors could not be found. One possibility is that a mixed oxygen environment is too complicated for the available data to determine. However, this is difficult to reconcile with the observation that the FT peak in this system is significantly shifted to larger R, given that Zn-O bond lengths are typically very similar. The increased strength of the FT peak and shift to larger R suggest the possibility of a larger, heavier neighbor, but a likely candidate is not clear. For instance, the FT peak from a Zn-Zn bond would peak at an R of ~2.3 Å, and a Zn-Fe bond would likely behave similarly. Determining the details of this structure will likely depend on the acquisition of additional data with an improved signal-to-noise ratio.

Discussion

Previous researchers have noted significant Zn-Fe second-nearest-neighbor interactions when Zn^{II} is bound to goethite via an inner-sphere (IS) complex or when Zn^{II} is coprecipitated with iron oxide minerals [3] . While our data may demonstrate a weak increase in second-order interactions upon microbial VHSA goethite reduction, we did not observe a strong M-M shell (i.e., Zn-Zn and/or Zn-Fe) in the Fourier-transformed EXAFS spectra. Thus, the incorporation of Zn^{II} into acid-insoluble moieties is difficult to interpret in the absence of a clear second-nearest neighbor. Furthermore, absence of a second-shell contribution is commonly interpreted as an indication of outer-sphere (OS) surface complexes. Since OS complexes are readily exchangeable, and since the Zn^{II} remains in an acid-insoluble form in these experiments, this OS interpretation cannot be correct. This conflict can be resolved only if Zn^{II} is becoming incorporated into an acid-insoluble metal oxide mineral goethite (but the extremely small iron oxide particle size, the presence of crystal defects, and/or the Zn/Fe molar ratio influences the EXAFS contributions by reducing longer-range [higher shell] interactions) or if Zn^{II} is becoming incorporated into a different acid-insoluble solid phase where a lighter compound, such as phosphorus or sulfur, provides a second-nearest neighbor.

The Zn K edge XANES spectra for sterile sediment MNC-71 suggests that sorbed Zn^{II} exists in an octahedral structure similar to that observed on the two goethite samples and that some degree of multiedge polyhedra exist (for example, see Ref. 4). Again, consistent with the goethite surfaces, the Zn EXAFS is best modeled by a split first shell of oxygen with a coordination number of 5. No evidence exists for higher shells in the sterile spectrum, again suggesting an absence of IS surface complex formation, in contradiction to the fact that some Zn^{II} remained insoluble in 0.5 M HCl. Upon reduction by *S. putrefaciens*, the near-edge spectra have the appearance of a tetrahedrally coordinated Zn environment, as evidenced by the presence of three near-edge features characteristic of such coordination. Qualitative comparison of XANES data for reduced-sediment MNC-71 with near-edge spectra of hydrozincite, ZnS, and $ZnCl_2$ standards (not shown) suggest that this shift in Zn^{II} coordination chemistry primarily results from the formation of $ZnCl_2$. These data also indicate that the multiple-scattering features observed at ~9690 eV in the inoculated MNC-71 XANES spectrum have an intensity similar to the intensities observed for ZnS or hydrozincite. This would suggest the formation of a longer-range structure, the degree of which is consistent with the two standard spectra. The chemistry, however, is clearly different. Since features due to multiple scattering can be attributed to multiple sources and are not predictive [4], the nature of phases other than $ZnCl_2$ remain indeterminate.

The $ZnCl_2$ interpretation is also supported by EXAFS model calculations, which yield the best fit to the experimental data with a $ZnCl_2$ structure. It is interesting that the fit is further improved by allowing Zn^{II} complexation with a small and indeterminate number of lighter atoms (indicated by removing the lower *k*-space region). This improvement may reflect some small contribution from oxygen. However, this EXAFS feature can also be attributed to other mechanisms such as (a) aqueous Zn^{II}, (b) IS and OS Zn^{II} surface complexes, or (c) a high degree of hydration within the $ZnCl_2$. Thus, any attempt to quantify this Zn-O contribution remains speculative at this juncture. The formation of $ZnCl_2$ is perplexing, since thermodynamic calculations provide little support for formation of this phase. Given the presence of Fe^{II} and Fe^{III} minerals and the

observed color changes, this moiety may also represent Zn^{II} association with some sort of poorly ordered, Cl^- green rust. However, the lack of second-shell Zn-M interaction argues against the formation of well-structured green rust.

Acknowledgments

Use of the APS was supported by the U.S. Department of Energy, Office of Science, Office of Basic Energy Sciences, under Contract No. W-31-109-ENG-38. The authors are also grateful for the help and support of the PNC-CAT staff.

References

[1] D.C. Cooper, F. Picardal, J. Rivera, and C. Talbot, Environ. Sci. Technol. **34**, 100-106 (2000).

[2] U. Schwertmann and R.M. Cornell, *Iron Oxides in the Laboratory: Preparation and Characterization* (Wiley-VCH, Weinheim, Germany, 1991).

[3] G.A. Waychunas, C.C. Fuller, and J.A. Davis, Geochim. Cosmochim. Acta **66**, 1119-1137 (2002).

[4] G.A. Waychunas, C.C. Fuller, J.A. Davis, and J.J. Rehr, Geochim. Cosmochim. Acta **67**, 1031-1043 (2003).